doi:10.20944/preprints202109.0278.v1

Article

Water-resistant surface modification of hydrophobic polymers with water-soluble surfactant additives

Colin P. Gibson [1], Matthew A. Litwinowicz [1], James P. Tellam[2], Rebecca J. L. Welbourn [2], Maximilian W. A. Skoda [2], Jan Claussen[3] and Richard L. Thompson [1,*]

1 Department of Chemistry, Durham University, Mountjoy Site, Durham, DH1 3LE
2 STFC ISIS Neutron and Muon Source, Rutherford Appleton Laboratories, 2;
3 Procter & Gamble, German Innovation Center (GIC), Sulzbacher Str. 40-50, Schwalbach am Taunus, Germany
* Correspondence: r.l.thompson@durham.ac.uk; Tel.: (+44 191 334 2139)

Abstract: Water-soluble nonionic surfactant, pentaethylene glycol monododecyl ether, $C_{12}E_5$, spontaneously blooms to the surface of spin-cast hydrophobic polyisoprenes, generating hydrophilic surfaces. This system represents a simple model for hydrophilic chemical modification of rubbery polymers yet demonstrates surprisingly rich, complex and unexpected behaviour. The vertical depth profiles were quantified using neutron reflectometry (NR) and deuterated surfactant, and the surface properties were characterized using contact angle analysis and atomic force microscopy (AFM). Despite the low surface tension of the toluene solvent used in film preparation and the low surface energy of the PI matrix, NR depth profiles revealed clear evidence of surfactant segregation. This surface layer was typically thicker than a monolayer, but incomplete, yet was remarkably stable with respect to dissolution, even when exposed to hundreds of thousands of times the volume of water required to dissolve all the surfactant on the surface. Despite the apparent resistance to removal from the surface, water exposure does alter the subsequent wettability of the surface, with a hydrophilic-to-hydrophobic transition occurring after rinsing. Complementary AFM images of these $C_{12}E_5$ / *cis*-PI films showed unexpected strand-like features on the surface of the film, which we attribute to a non-uniform lateral distribution of some of the surfactant. This surface structure becomes more evident after rinsing, and it appears that there are two distinct populations of surfactant on the PI film surface. We conclude that some of the bloomed surfactant exists as layers, which are relatively inert with respect to rinsing or surface modification, and some is laterally inhomogeneous. This latter population is primarily responsible for surface wetting behavior, but is not detected by specular NR.

Keywords: Surface modification; hydrophobicity; blooming; segregation; surfactant; poly(isoprene)

1. Introduction

Polyisoprene, PI, is a key component of many industrial and consumer products; it is the main component of natural rubber, for which global annual production is around 10,000,000 tons[1,2]. However, for many applications, polymers need surface modification to satisfy requirements such as wettability, anti-fouling or adhesion. Techniques to modify surfaces [3–7] can be divided into physical and chemical techniques[2,8] and can help to impart desirable surface properties.

Physical surface modification techniques involve the modification of the matrix polymer itself. These techniques include plasma[9] and ozone treatments[10], as well as flame and corona treatment methods. While these techniques can selectively modifying specific areas of the surface, they introduce additional steps into the manufacturing process and frequently have high energy requirements. Furthermore, when used to generate hydrophilic surfaces, the benefits are often only temporary, with the polarised surfaces rearranging to minimise the surface energy[11]. This is likely to be particularly problematic for rubbery polymers such as PI, because of the high mobility of the polymer chains at ambient temperatures.

Chemical surface modification relies on the introduction of additive molecules to a polymer. Successful surface modification requires the delivery of these additives at the surface, which in turn requires some extent of segregation or demixing normal to the surface. The demixing of the two molecules is governed by the balance between the energetics of the interactions between the two components as well as the entropy of the formation of a segregated system[12–14]. Highly branched additives have shown promise in laboratory scale tests, where the partitioning of chain ends to the surface has been shown both experimentally[15,16] and computationally[17–19] to be entropically favoured.

While it is relatively straightforward to generate hydrophobic surfaces, hydrophilic surfaces are more challenging to form, because hydrophilic moieties usually have a high surface energy, which inhibits their surface segregation. Usually, small differences in surface energy along with incompatibility are most significant in directing and promoting surface segregation.[20–22]. Previous methods to achieve this surface segregation have involved the use of amphiphilic additives, which combine low surface energy groups or low molecular weight to promote surface segregation, along with polar groups that could offer a hydrophilic surface property[23,24].

Surface modification of polyisoprene with amphiphiles has received relatively little attention,[25] and we are unaware of any, which study this behaviour from a molecular scale perspective. There is, however, strong evidence of surface segregation of non-ionic surfactant in polypropylene[24,26–30], a more crystalline polymer than *cis*-PI. It has been shown that the structure of the additive molecule affects the migration of the additive. Additives with a larger hydrophilic group (and thus greater HLB value) produce a larger surface layer[31]. However, the rate of surface migration becomes slower with increasing hydrophilic group size, possibly because this size hinders diffusion through the matrix to the exposed surface. We note that other contributing factors such as a greater tendency of larger molecules to form aggregates may also hinder the dynamics of surface segregation.

Datla *et al*.[31] reported XPS results, which also showed surface segregation of non-ionic surfactants on polypropylene surfaces, and interestingly, the hydrophilicity enabled by the surfactants additive changed with ageing. For some surfactants, hydrophilicity increased with time, whereas for other surfactants this surface modification decreased with time. Unfortunately, it was not possible to resolve the composition profile either vertically or laterally, so it was not possible to relate changes in surface modification to the underlying structure of the adsorbed surfactant.

Here, we consider a model system of a hydrophobic polymer, *cis*-polyisoprene "*cis*-PI" and surfactant additive, pentaethylene glycol monododecyl ether "$C_{12}E_5$". By using a simple single-component surfactant, it is possible to interpret nano-scale organisation and the blooming process at a molecular level and eventually use this understanding to improve the efficiency of chemical modification techniques. We explore the relationship between surface modification and the organisation of the adsorbed surfactant for the first time, by combining neutron reflectivity (NR) and AFM, to resolve the precise vertical and surface lateral distribution of the surfactant in or on the polymer. We further consider the resilience of the surface modification and the underlying surfactant structure by studying the same films with these techniques after heating and after rinsing, which are necessary steps towards understanding how to achieve surface modification efficiently.

2. Materials and Methods

Materials and sample preparation

Cis-Polyisoprene $T_m \sim 24$ °C, $T_g = -65$ °C, (See supporting information Figures S1 and S2) (Sigma-Aldrich, 97% *cis*-1,4) and $C_{12}E_5$ (Aldrich) were purchased and used as received. Deuterated $C_{12}E_5$ (d_{25}-$C_{12}E_5$) was synthesised at the Rutherford Appleton Laboratories as described elsewhere[32]. Films were spin-cast onto clean silicon wafers, which were first washed with acetone to remove hydrophobic impurities. *Cis*-PI was dissolved in toluene by heating to 50 °C with stirring to yield 4% (w/w) solutions. $C_{12}E_5$ and d_{25}-$C_{12}E_5$ were also dissolved in toluene to make 10 % (w/v) solutions. These solutions were then mixed and further diluted with toluene to yield 2% (w/w) solutions with the desired proportions of polymer and surfactant. Deuterium-labelled d_{25}-$C_{12}E_5$ films were used for neutron and ion beam experiments and hydrogenous samples used for all other experiments. The mixed solutions were heated to 60 °C and spin-cast onto silicon wafers that had been pre-heated to approximately 80 °C. Heating was necessary to avoid the solution de-wetting the substrate during spin-coating. The evaporation phase of spin coating was completed within 30 s. Films were prepared in the same way for NR except silicon blocks with 55 mm diameter and 5 mm thickness were used as substrates instead.

Neutron Reflectometry

Neutron reflectometry (NR) has been extensively used for studying structural organisation of soft matter[33–38]. This technique is advantageous when studying soft matter as it is possible to conduct experiments at atmospheric pressure and has a vertical resolution (~0.5 nm, limited by the beam collimation and the size of the silicon blocks used) capable of resolving structure changes on the molecular scale. Concentration versus depth profiles were obtained using the INTER reflectometer at the Rutherford Appleton Laboratories, UK. Deuterium labelling provided contrast between layers within the sample by utilising the difference in scattering length density (SLD) of the components. The SLDs of each component of the films and substrates are given in Table 1. A momentum transfer (Q) range of $0.005 < Q/\text{Å}^{-1} < 0.3$ was collected to give a complete reflectivity curve. This range requires measurements at 3 angles and has a significant collection time (~1.5 h per sample). Samples were heated using a temperature-controlled stage and were rinsed under flow of ultrapure water (resistivity: 18.2 MΩ cm) for 10 s. For some samples the rinsing process was repeated for an additional 10 s and the reflectivity measured after a total of 20 s rinsing. Analysis of all reflectivity was performed using MUSCtR.[39] This software allows for the gradual variation in film thickness present in some films, by fitting of multiple depth profiles (Figure S3, Supplementary Information Section) to a single set of data. These depth profiles are identical except for a defined variation in thickness of the bulk layer thickness, ± 250 Å, to approximate the macroscale film thickness undulations. Combining calculated reflectivities in this way suppresses the Kiessig fringes, whilst maintaining the overall shape of R(Q), which cannot be achieved by increasing the interlayer roughness for a single composition profile.

Nuclear Reaction Analysis

Nuclear reaction analysis (NRA) is a real-space depth profiling technique, which can yield similar composition versus depth profiles to neutron reflectometry. NRA was used to assist the interpretation of NR data by providing unambiguous composition profiles, albeit at lower resolution. A 2 mm diameter 0.7 MeV beam of $^{3}He^{+}$ ions was used at a grazing incidence of 70° to the sample normal, to induce nuclear reactions with the deuterons of the d_{25}-$C_{12}E_5$. Data were summed from measurements over several 6 × 2 mm elliptical patches. Backscattered protons were detected at 170° to the incident beam. The NRA technique and instrument setup used are discussed in greater detail elsewhere.[30] Data were fitted using Datafurnace Software[40,41]. Typical data, fits and derived concentration profiles are given in supplementary information, Figure S4.

Table 1. Scattering Length Densities for Hydrogenous and Deuterated Components

Component	SLD / 10^{-6} Å^{-2}	Density / g cm^{-3}
cis-PI	0.26	0.91
d_{25}-$C_{12}E_5$	3.60	0.963
Si	2.07	2.33
SiO_2	3.47	2.56

Atomic Force Microscopy

The surfaces of spin-cast films were analysed using a Bruker Multimode 8 scanning probe microscope in PeakForce quantitative nanomechanical mapping mode (QNM) to map variations in height and mechanical properties simultaneously. Using a J-type scanner, 30 × 30 µm areas of each sample were scanned, capturing images with 512 points per line. NuNano Scout 70R probes with a spring constant of 2 N m^{-1} and resonant frequency of 70 kHz were used. Height map data were then flattened using Gwyddion (v2.53) to remove natural curvature caused as the sample is moved relative to the cantilever. AFM was also used to characterise total film thickness by measuring the height difference between the film surface and the substrate where the film was removed by scratching.

Water Contact Angle Analysis

Contact angle measurements were made using the sessile drop technique with a contact angle goniometer. Images were recorded using a digital camera equipped with a telecentric lens to remove the effects of the depth of field. A 5 μL droplet of the probe liquid (ultrapure water) was placed on the spin-cast film surface and a video of the droplet was recorded. Frames were extracted from the video at regular time intervals and analysed using the DropSnake plugin within ImageJ[42].

3. Results

Additive segregation

NR results are presented as volume fraction depth profiles (Figure 1). The surface excess provides a convenient measure of the total amount of segregated surfactant at the exposed surface. Here, we define the surface excess, z*, which is equivalent to the thickness of a pure layer of surfactant, as

$$z^* = \int_0^\infty \varphi(z) - \varphi_\mathrm{b}\,\mathrm{d}z \qquad (1)$$

where $\varphi(z)$ is the concentration at depth z and φ_b is the bulk volume fraction. This measure of the surface excess is related to the area per adsorbed molecule, more commonly used in the surfactant science literature, *Γ*, by

$$\Gamma = z*/v_{surf} \qquad (2)$$

where v_surf is the volume of the surfactant, ~701 Å^3.

Figure 1 and **2** present the concentration dependence of the surfactant in the near-surface region of the film. The total film thickness measured by AFM was 4500 - 6000 Å; therefore too thick to characterise directly by NR. We found clear evidence of d_{25}-$C_{12}E_5$ blooming of the surfactant to the surface, of PI films, both below and above the melt temperature of PI. In all cases the films are well above their T_g of ~-65 °C, Figure S3. The surface segregation is also clearly evident, even at lower resolution by Nuclear Reaction Analysis, Figure S3. Whilst the bulk shows a concentration consistent with the expected average surfactant loading, there is a much larger concentration present near the surface. As the average concentration increases, the surface layer also becomes thicker and more enriched. However, the maximum surface concentration of the surfactant is significantly less than 100% and the surfactant instead presents as an enriched layer in the depth profile. This enriched surface layer is also confirmed in nuclear reaction analysis depth profiles, where a layer of d_{25}-$C_{12}E_5$ is also present (Figure S4). Computational studies have calculated the length of a $C_{12}E_5$ molecule to be approximately 28 Å in a vacuum[43]. This molecular length represents the maximum thickness of a monolayer: whilst the thickness can be decreased by folding or tilting of the molecule, it cannot exceed this length. It is clear that the adsorbed surface layers are much thicker than the length of a single molecule, Figure 1. Furthermore, samples of 10% surfactant loading show a surface excess of 36 Å (**Table 2**), which exceeds the maximum quantity of surfactant that could exist as a single layer. Our results clearly show that while it is commonly the case that there is sufficient bloomed surfactant on the film surfaces to form a pure monolayer, it takes the form incomplete multi-layers with a surface concentration of 60% surfactant or less.

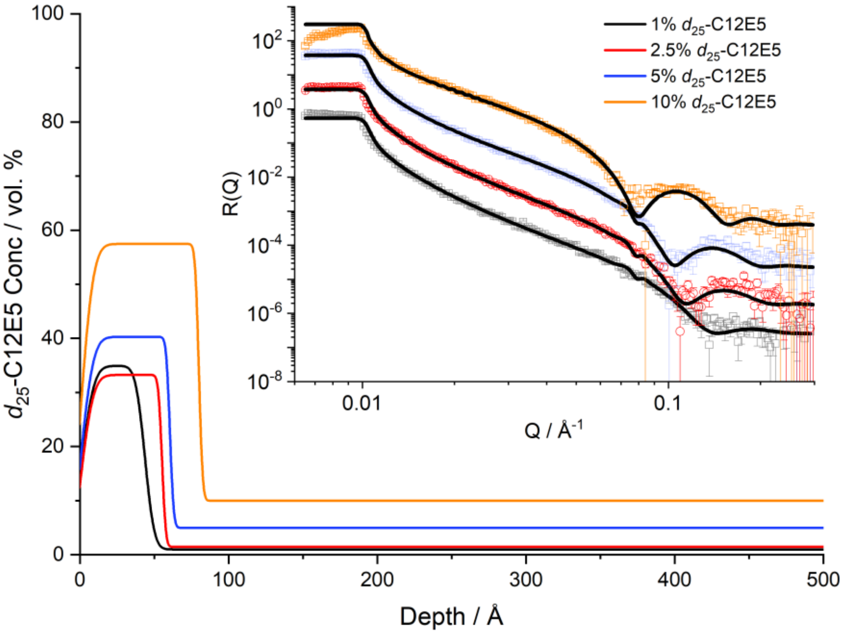

Figure 1. Near-surface concentration profiles of d$_{25}$-C$_{12}$E$_5$ in *cis*-PI at 20 °C. Reflectivity data and fits are shown in the inset, offset for clarity.

Table 2. Surface excess for samples at 20, 45 and 60 °C and after rinsing for 10 s and 20 s with deionised water. NR data and fits used to obtain depth profiles are presented in figures S5,6,7 and 8.

[d$_{25}$-C$_{12}$E$_5$] / wt%	z* / Å				
	20 °C	45 °C	60 °C	20 °C, 10s rinse	20 °C, 20s rinse
1	14	13	14	13	14
2.5	16	17	14	11	11
5	15	17	18	13	14
10	36	34	33	30	34

The Effect of Temperature Elevation on the Surface Excess

Upon heating, the surface excess shows very little change, Table 2. The uncertainty of surface excess measurements is 1-3 Å, [44] thus, there is no evidence for the surface excess measurements given in having any significant temperature dependence. The concentration profiles from which *z** values were derived are shown in figure 2. Although there appear to be some small variations in the calculated profiles, these are close to the limit of precision of the measurement, and there is no systematic shift in the surface concentration or thickness of the adsorbed layer with changing temperature. We note that in this temperature range, none of the film components are solid or glassy; therefore samples should be relatively unhindered in approaching equilibrium.

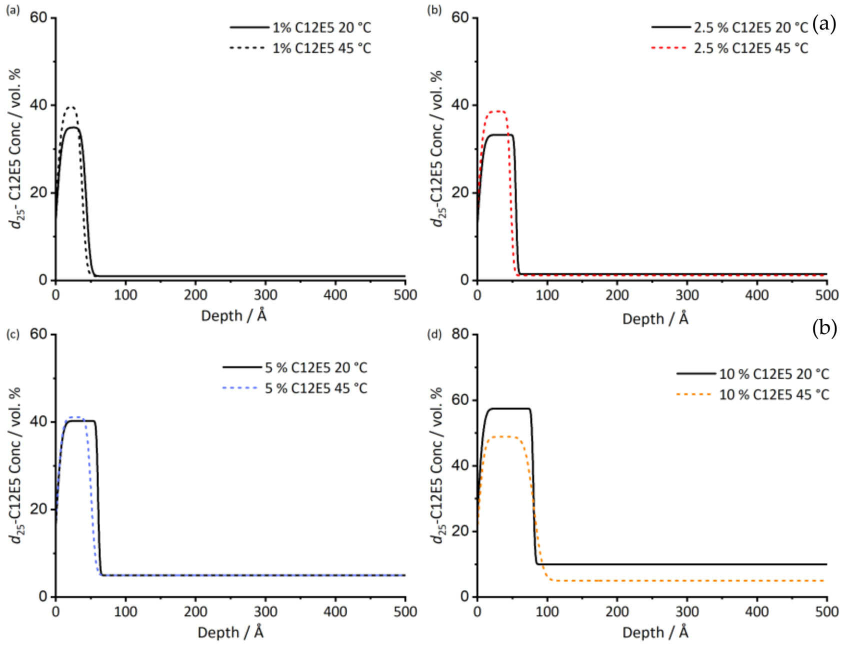

Figure 2. Depth profile of cis-PI / d_{25}-$C_{12}E_5$ films at both 20 and 45 °C. The depth profiles are determined from the scattering length density profiles of the films. Surfactant loadings are 1 % (a), 2.5 % (b), 5 % (c), 10 % (d). Fitted data used to obtain 45 °C depth profiles are given in Figure S5.

Water Exposure Effects on the Surface Excess

The surface segregation of d_{25}-$C_{12}E_5$ was quantified using NR at 45 °C and 60 °C and then after repeated 10 s rinses with ultrapure water and these surface excess measurements are summarised in **Table 2**. Rinsing once or even twice causes surprisingly little change in surface excess: the largest change shown upon rinsing is in the 5% surfactant sample, with a decrease of ~27 % (between 60 °C and re-measured at 20 °C after a 10s rinse). When compared to the uncertainty of these measurements, noting the slightly higher values recorded after a second rinse, there is again remarkably little change in surface excess concentration upon rinsing.

Wahlgren *et al.* [45] determined the solubility of $C_{12}E_5$ to be in excess of 10 w/v% (based on cloud point). From this value, for a single rinse of approximately 10 mL of water, 1 g of $C_{12}E_5$ could be dissolved. Based on the surface excess thickness for 1% $C_{12}E_5$ loading a 55 mm diameter silicon block will have 3.2 μg of surfactant at the surface. This would only require 32 nL of water to dissolve, meaning that there is over 300,000 times the amount of water present that is required to remove all of the surface layer at equilibrium. If all of the surfactant was capable of moving from the film into the water, it would be reasonable to assume that all surfactant would be removed from the surface: the surface layer is thin and so there is little to prevent surfactant loss. However, the post-rinsing NR results for the surface excess, summarized in Table 2 indicate that the surfactant / polymer film is remarkably stable with respect to rinsing. Further rinsing for an additional 10 s appears to have no significant effect on the surfactant distribution.

Water Contact Angle Analysis

Our water contact angle (WCA) results show that significant levels of hydrophilicity are generated in films containing at least 5% $C_{12}E_5$ surfactant. It is interesting to note that while the surface excess measured by NR at 5% surfactant is similar to results for lower loadings of surfactant, there is a significant change in WCA over this range.

Whilst the NR data shows that the adsorbed surfactant is stable with respect to water exposure, the contact angle data presented in **Figure 3** presents equally clear evidence that the surface properties are dramatically modified by rinsing. It should be noted that contact angle measurements show significant (several degrees, figure S9) variation, when repeat measurements are carried out, even when on nominally identical samples. Thus, we treat individual results with caution, while noting the following points: In the as-made samples, there is no significant surface modification at 1% $C_{12}E_5$ compared to the 0% control sample. Contact angles are relatively independent of time, only decreasing after periods of >100s, at which point evaporation of the contacting droplet gives rise to a receding contact angle, which is lower than the initial advancing contact angle. At higher (5%, 10% $C_{12}E_5$) loadings, film surfaces are much more hydrophilic and contact angles decrease with time over short periods. It is expected that the hydrophilicity of the films will depend on the presence of $C_{12}E_5$ on the surface of *cis*-PI, which is otherwise hydrophobic. After rinsing, the contact angles increase for all compositions, and in some cases (1 and 10% $C_{12}E_5$) show contact angles greater than 90°. When comparing the results from NR and contact angle analysis, there is evidence for incomplete surface coverage: NR shows there is a layer enriched in surfactant for all samples, yet not all samples show wetting behaviour when water is placed on the surface. This is indicative of domains of surfactant on the surface with other regions of exposed *cis*-PI.

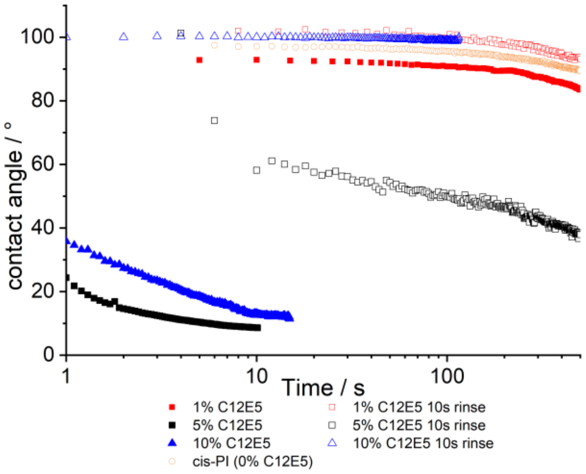

Figure 3. Contact angles for cis-PI films containing between 1 and 10% $C_{12}E_5$ both before and after a 10 s rinse with deionised water. The data is a function of time where 0 is the time that the probe droplet (water) is placed on to the surface. A *cis*-PI sample has also been shown in orange, showing 0% surfactant loading.

Surface structure change after water exposure

AFM measurements are shown in Figures 4, 5 and 6 with height and adhesion maps presented. The AFM images confirm the presence of gradual undulations in film-thickness, which necessitated multi-profile fitting of the NR data. Before rinsing, a small number of thread-like “strand” features were found on the surface. These strands are slightly raised with respect to the surface and correlate with regions of increased adhesion. In the absence of any variation in composition, raised features usually correlate with a reduction in adhesion due to the reduced contact area between the probe and the surface. Here, the increase in adhesion on these raised features indicates that the strands are of a different composition from the surrounding surface, most likely the surfactant.

The strands become more apparent at higher concentrations, with strands appearing in the adhesion surface maps above 2.5% before rinsing. The strands also become more pronounced after rinsing for 10 s, with more strands appearing on the surface after rinsing. It is important to note, however, that images do not show the same position on each sample. As the sample is removed from the AFM to be rinsed, it is not possible to return the sample to the same position upon reintroducing it to the microscope. However, the trends observed are consistent across all samples.

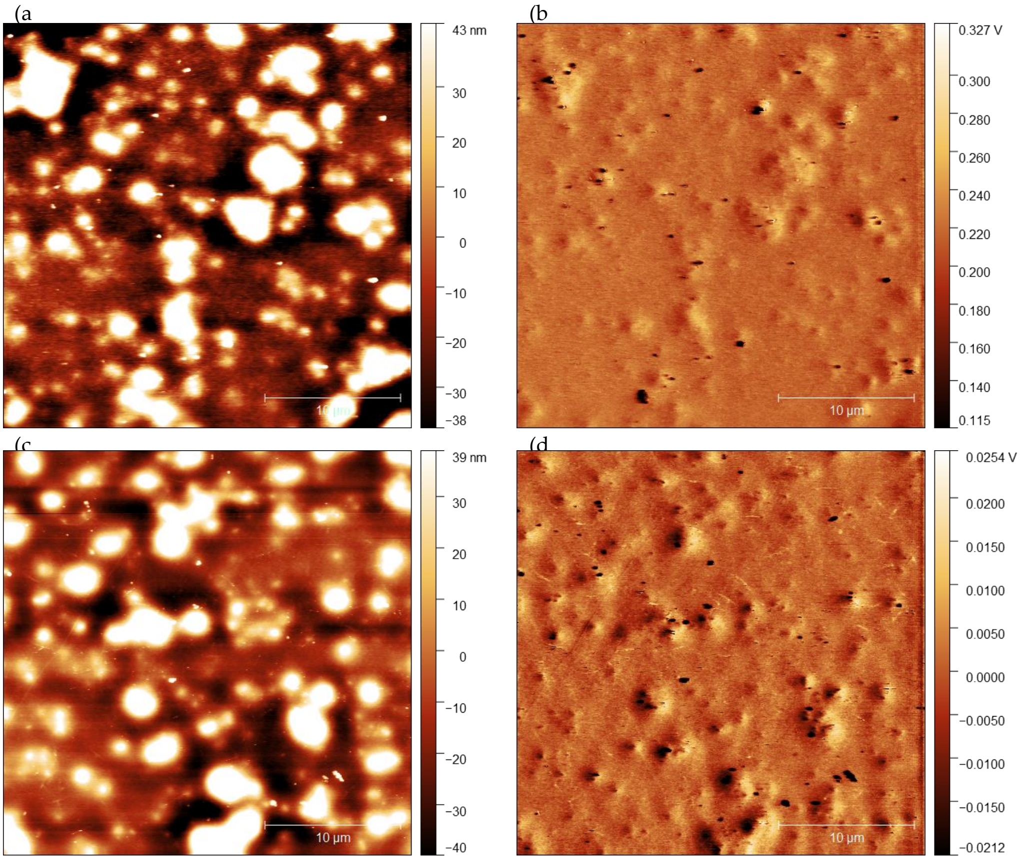

Figure 4. (a) AFM height map of cis-PI films with 1% loading of $C_{12}E_5$ and (b) Adhesion maps for the same position on the same film; (c) height map of the same film shown in the top AFM images after 10s rinse and (d) the adhesion map.

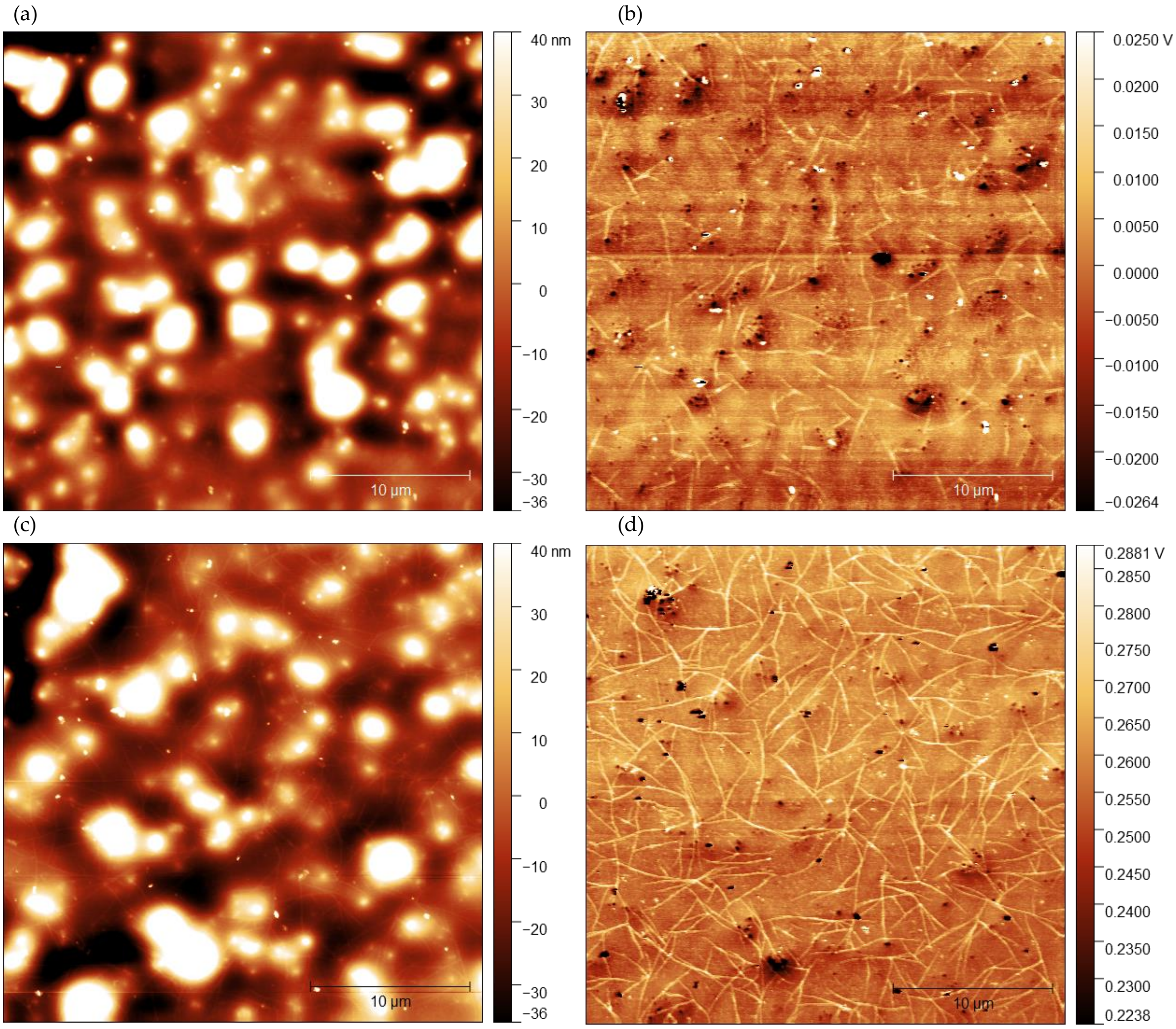

Figure 5. (a) AFM height map of cis-PI films with 2.5% loading of $C_{12}E_5$ and (b) Adhesion maps for the same position on the same film; (c) height map of the same film shown in the top AFM images after 10s rinse and (d) the adhesion map.

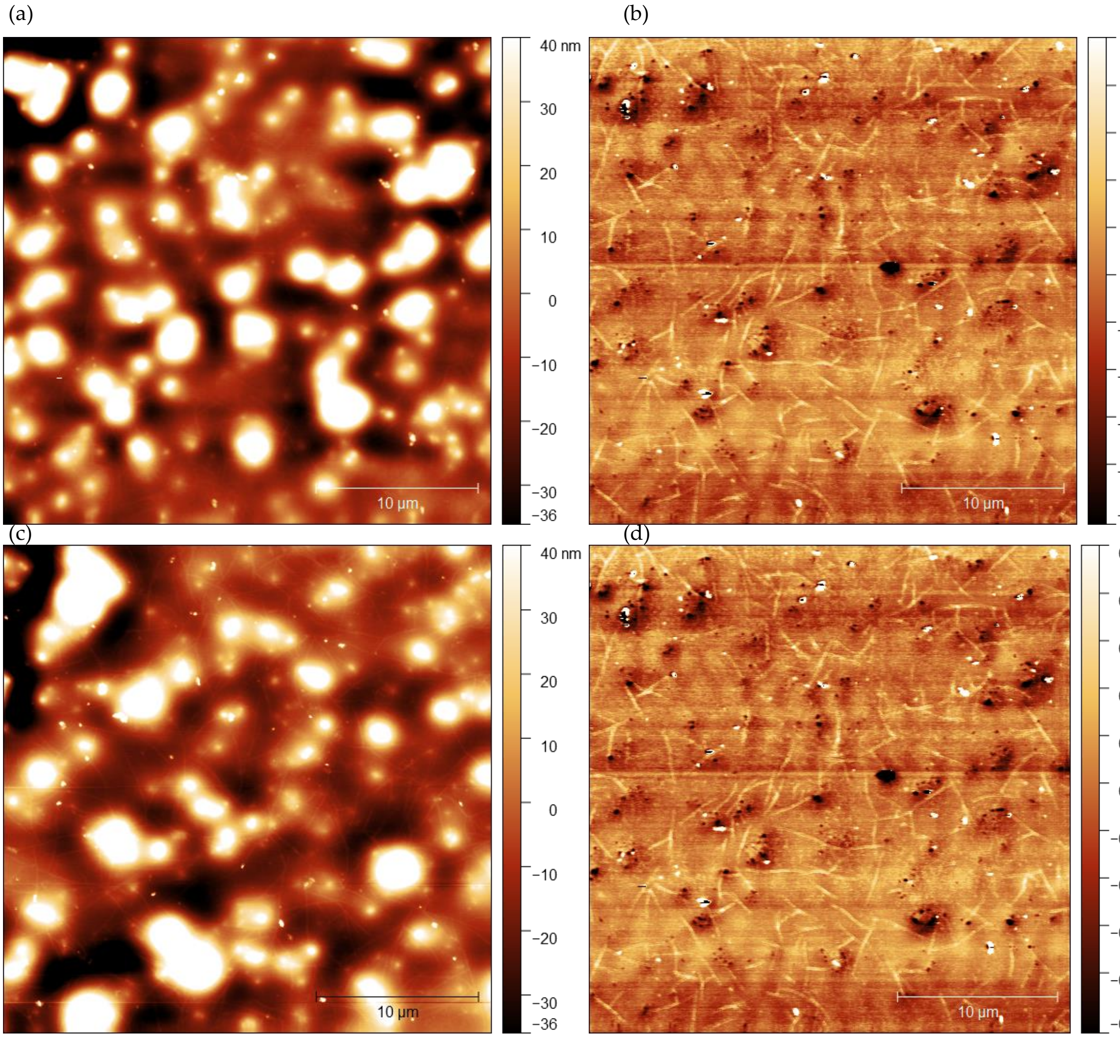

Figure 6: (a) AFM height map of cis-PI films with 10% loading of $C_{12}E_5$ and (b) Adhesion maps for the same position on the same film; (c) height map of the same film shown in the top AFM images after 10s rinse and (d) the adhesion map.

4. Discussion

Surfactant Blooming

There are few literature examples of hydrophilic additives being used to within non-polar polymers. Whilst Zhu and Hirt reported the formation of a surface layer of hydrophilic additives present on a hydrophobic polypropylene film [24], this work could not resolve the precise thickness of this surface layer because of the more limited depth resolution of ATR-FTIR used. Nevertheless, it appears that hydrophilic modification is possible, not only in the molten extruded films of Zhu and Hirt's study, but also in spin cast films that we consider here. This similarity suggests that the preparation technique and particularly the presence of solvent in sample preparation does not hinder the migration of an additive molecule.

Studies by Briddick *et al*.[46] in polyvinyl alcohol films showed surface layers of $C_{12}E_5$ present with a thickness that is comparable to the thicknesses reported in **Figure 1**, suggesting that the initial surfactant segregation is similar in both PVA and *cis*-PI matrices. The surface segregation in *cis*-PI is much less expected than in PVA: The PVA films were spin-cast from water in which these surfactants are highly surface-active, but these PI films are spin-cast from toluene, with a low surface energy and so no surface activity of $C_{12}E_5$ is expected. Furthermore, the surface energy of PI (32 mN m^{-1}) [47] is lower than that of PVA (37 – 59 mN m^{-1})[48–50], again indicating a lower thermodynamic impetus for surface segregation.

The thickness of the enriched surface layer is well-characterised by NR and presents evidence of a multilayer structure. Multiple (even number) layers of surfactant would allow the surfactant to present the hydrophobic, low surface energy groups to both the hydrophobic polymer and the air. Whilst an even number of layers could present a low energy surface to both the air and bulk polymer, when exposed to water, only an odd number of layers would maintain the arrangements at the *cis*-PI whilest presenting a hydrophilic surface to the water interface. It is interesting to note that the smallest layer thickness observed is ~ 40 – 50 Å, corresponding to a bilayer structure, possibly tilted. Furthermore, the 10% sample shows a surface layer that is nearly 100 Å thick, corresponding closely to a 4-layer structure. No samples show a surface layer with a thickness between these values, suggesting that a 3-layer structure is unstable. Such a structure would have to present polar oxyethylene surfaces against the non-polar *cis*-PI or exposed to air, neither of which would be energetically favourable. The small discrepancy between the measured layer thicknesses and even multiple of the extended surfactant chain length indicates some tilting of the surfactant molecule orientation with respect to the sample normal, or possibly some overlap or interdigitation between layers.

Although the temperature dependence of surfactant segregation in polymers has received relatively little attention, we can draw some useful comparison between our experiments and previous reports on the behaviour of plasticisers in polymers. Xie *et al.*[51] investigated surface segregation of dioctyl phthalate (DOP) to the surface of polystyrene (PS) films. They found that heating samples after film preparation caused an increase in the surface DOP concentration up to 60 °C, after which surface DOP concentrations decreased. The samples were below the T_g of PS in this example, and heating towards the T_g, likely favours the equilibration of the DOP, promoting segregation. However, because the *cis*-PI samples are far above their T_g, heating has little effect on the vertical distribution. The absence of any strong temperature-dependence in these films suggests that heating has little impact on the thermodynamic favourability of adsorption over this range.

The concentration-independence of z^* is unexpected for an incompatible surfactant that forms multilayers on the film surface. Previously, we have found that highly compatible amineoxide surfactants in PVA form a concentration-independent surface excess, but the segregation of other, less compatible surfactants is strongly dependent on concentration.[44] In the case of compatible mixtures, z^* and the thickness of the adsorbed layer corresponded closely to a surfactant monolayer [44]. Here, however, the multilayer adsorbate is not consistent with a compatible surfactant and as such, we would expect the amount of surfactant excluded to the surface to increase with increasing bulk concentration.

The fraction of surfactant within the entire film that appears as an enriched layer is also a useful metric to assess. This fraction can be defined by equation 3, where φ_{surf} is the surface fraction, z^* is the surface excess and φ_{total} is the total amount of surfactant within the film of thickness, L.

$$\varphi_{\text{surf}} = \frac{z^*}{L\varphi_{\text{total}}} \tag{3}$$

Table 3: surface fractions for *cis*-PI / $C_{12}E_5$ at 20 °C.

Film surfactant loading / wt. %	φ_{surf}
1	0.21
2.5	0.20
5	0.08
10	0.07

Throughout the composition range studied, the majority of the surfactant remains in the bulk of the film, Table 3. This observation indicates that the surface modification is not very efficient at a molecular level for these materials and concentration range, but it does allow for the possibility that the remaining surfactant in the bulk could later be exploited to regenerate a hydrophilic surface. Such a process might be possible if further surface segregation could by triggered by some stimulus, such as heating.

When considering the effect of temperature elevation, it is important to consider the effect of evaporation of the surfactant on the distribution. This is because the combination of a minute sample volume (~0.1 mg) with a macroscopic surface area (~10 cm^2) in these spin-cast films provides an ideal geometry to promote evaporation. In a similar thin-film geometry, Smith *et al.*[47] showed that for a small molecule (a plasticiser) in a polyester/polyurethane film, the rate of loss of the surfactant is limited not by the rate of diffusion of the molecule in the film, but by the rate of evaporation of additive from the film. We note for our purposes that if the rate of evaporation were significant compared to the rate of diffusion within the film, then the near-surface region of the film would be depleted, rather than enriched in surfactant as we found. Furthermore, we find that even after equilibrating samples at 45 °C for approximately 8 hours, the changes in the composition profile are negligible; therefore there is no evidence for evaporation during heating.

Surface Structures

When the hydrophobic surfaces observed in contact angle measurements are compared with the surface excesses before and after rinsing, there is evidence for molecular reorganisation following initial exposure to water to render the surface more hydrophilic, but after this exposure, the surface then becomes quite hydrophobic with respect to further contact with water. This suggests some further rearrangement after drying, from which the surfactant is then unable to reorganise into a hydrophilic coating when the contact angle experiment is repeated after rinsing. $C_{12}E_5$ has previously been shown to form lamellar structures at high concentrations in water[52]. Whilst the substrate on which these structures form is significantly different, with a liquid interface compared to a polymer, it is possible that a similar structure forms at the surface of the polymer, minimising contact of hydrophilic head groups with a low surface energy polymer, whilst also presenting a low surface energy interface to the air.

The precise origin of the surface changes as seen in Figure 4, 5 and 6 is unclear, but is consistent with some change in the organisation of the surfactant. While strand-like features of $C_{12}E_5$ adsorbed on mica surfaces under water have been reported by Dong and Mao[53], we are unaware of any similar behaviour reported as spontaneously forming at the solid-air interface. In our work, the strands that spontaneously form are much longer than have previously been reported on surfaces and are unusual that they are essentially free-standing, do not exist in arrays, and are not obviously altered by rinsing. We note that although these surface features are much straighter, the length of the strand features is consistent with the worm-like micelles of $C_{12}E_5$ found in solutions by light-scattering studies[54].

Our results show an interesting discrepancy between the surface excess measured by NR, which is remarkably stable with respect to rinsing, and the wettability behaviour, which is altered by rinsing. The fact that repeated rinsing has no significant effect on the surface layer measured by NR suggests that it remains in place rather than is removed, then replaced from the bulk. Had the latter process occurred, we would expect that with two rinses, there would be a systematic depletion in any regernerated surface layer. Overall, our results indicate that the resilient surface excess measured by NR is not entirely responsible for the observed wetting behaviour. Interestingly, the surface excess measured by nuclear reaction analysis, 69Å, is almost twice the value measured by NR. We postulate that this discrepancy arises because the film surface includes some $C_{12}E_5$ that is detected by NRA, but not NR, and it is this fraction of the segregated surfactant that is mainly responsible for the wettability phenomena. The contribution to the surface excess that is only detected by NRA is most likely to arise from the ‘strands’ that are detected by AFM, and may also account for the anomalous concentration dependence of the surface excess noted earlier. These strands are relatively small (several microns) and are likely to be smaller than the coherence length of the neutrons, meaning that very little of the NR profile observed arises from incoherent addition.

5. Conclusions

We have shown that for spin-cast $C_{12}E_5$/*cis*-PI blends, a rich variety of complex and intriguing blooming behaviour is found. A clear surface excess of the amphiphile presents at the air interface, which is nearly invariant over a significant range of composition and temperature. There are few precedents for amphiphile segregation at hydrocarbon polymer surfaces[55,56] and neither concentration or temperature dependence of adsorbed nanostructures nor their stability with respect to rinsing have previously been reported. Our work shows that even when these blends are spin-cast from a low surface energy solvent, non-ionic surfactant adsorption is spontaneous, showing that this behaviour is more general than was previously known. We have also demonstrated that the non-ionic surfactant, which adsorbs to the surface is resistant to evaporation, with a surface excess remaining after temperature elevation for several hours.

The NR depth profiles presented indicate that surface adsorption is persistent even after exposure to significantly more water than is required to remove the surfactant. However, the contact angle measurements of the films before and after rinsing indicate a change in the surface properties of the film, indicating that there must be a structure change in the surfactant that occurs upon exposure to water. We can resolve this difference in observations by recognising that NR is only sensitive to planar structures such as complete surface layer. Other surface features such as strings and droplets may be invisible to NR, meaning that if these structure changes are induced upon water exposure, we may see little evidence of these features in NR, even though NR provides a very precise characterisation of surfactant bloomed on polymer surfaces. Only by a combination of techniques can an accurate picture of the blooming process be obtained, and it is apparent that this level of detail is needed in order to understand why such a complex relationship between surface segregation and surface modification exists.

Supplementary Materials: The following are available online at www.mdpi.com/xxx/s1, Figure S1: DSC Thermogram of cis-PI heated at 10 °C per min. The peak with a maximum at 24.38 °C shows the melting transition of the cis-PI, Figure S2: Raw DSC data of cis-PI, showing the glass transition at -65.08 °C, calculated from the extrapolated half C_p point, Figure S3. (a) sld profile for 1% $C_{12}E_5$ in cis-PI at 20 °C illustrating how the data is fitted. The three sld profiles shown have different bulk layer thickness and the difference in thickness between each profile is 250 Å. (b) The averaged predicted reflectivity profile from each of these model sld profiles, which was fitted to the experimental data, Figure S4. Nuclear reaction analysis depth profile of 10% d_{25}-$C_{12}E_5$ in cis-PI showing a surface excess. Inset: Fitted NRA data used to obtain the depth profile, Figure S5. Two successive measurements of contact angle on distinct locations on a single 1% $C_{12}E_5$ / cis-PI sample. Figure S6. NR data and fits for 1 to 10% d_{25}-$C_{12}E_5$ in cis-PI at 45 °C., Figure S7. NR data and fits for 1 to 10% d_{25}-$C_{12}E_5$ in cis-PI at 60 °C., Figure S8. NR data and fits for 1 to 10% d_{25}-$C_{12}E_5$ in cis-PI after a 10s rinse., Figure S9. NR data and fits for 1 to 10% d_{25}-$C_{12}E_5$ in cis-PI after a 20s rinse.

Author Contributions: Conceptualization, R.L.T. and J.C.; software (MUSCtR), M.A.L.; formal analysis, CPG.; data curation, CPG, JT, RJLW, MWAS.; writing—original draft preparation, review and editing, CPG and RLT.; supervision, RLT. All authors have read and agreed to the published version of the manuscript.

Funding: This research was funded by EPSRC/Procter and Gamble (UK) via EP/P007864/1 and the Soft Matter and Functional Interfaces CDT (SOFI-CDT) via EP/L015536/.

Data Availability Statement:. Data for the neutron reflection experiments is available at https://doi.org/10.5286/ISIS.E.RB1910298.

Acknowledgments: We thank Mr W.D. Carswell, Durham University, for the supporting thermal analysis (DSC) experiments.

Conflicts of Interest: The authors declare no conflict of interest.

References

1. Wolf, S.; Plenio, H. On the Ethenolysis of Natural Rubber and Squalene. *Green Chemistry* **2011**, *13*, 2008–2012, doi:10.1039/c1gc15265c.
2. Chan, C.H.; Joy, J.; Maria, H.J.; Thomas, S. CHAPTER 1. Natural Rubber-Based Composites and Nanocomposites: State of the Art, New Challenges and Opportunities. In *Natural Rubber Materials: Volume 2: Composites and Nanocomposites*; Thomas, S., Chan, C.H., Pothen, L., Joy, J., Maria, H., Eds.; The Royal Society of Chemistry, 2013.
3. Johnsen, K.; Kirkhorn, S.; Olafsen, K.; Redford, K.; Stori, A. Modification of Polyolefin Surfaces by Plasma-Induced Grafting. *J. Appl. Polym. Sci.* **1996**, *59*, 1651–1657.

4. Friedrich, J.; Wettmarshausen, S.; Hennecke, M. Haloform Plasma Modification of Polyolefin Surfaces. *Surface and Coatings Technology* **2009**, *203*, 3647–3655, doi:10.1016/j.surfcoat.2009.05.050.
5. Bongiovanni, R.; Di Gianni, A.; Priola, A.; Pollicino, A. Surface Modification of Polyethylene for Improving the Adhesion of a Highly Fluorinated UV-Cured Coating. *European Polymer Journal* **2007**, *43*, 3787–3794, doi:10.1016/j.eurpolymj.2007.06.037.
6. Mathieson, I.; Bradley, R.H. Improved Adhesion to Polymers by UV/Ozone Surface Oxidation. *International Journal of Adhesion and Adhesives* **1996**, *16*, 29–31, doi:10.1016/0143-7496(96)88482-X.
7. Chan, C.M.; Ko, T.M.; Hiraoka, H. Polymer Surface Modification by Plasmas and Photons. *Surface Science Reports* **1996**, *24*, 1–54, doi:10.1016/0167-5729(96)80003-3.
8. Nemani, S.K.; Annavarapu, R.K.; Mohammadian, B.; Raiyan, A.; Heil, J.; Haque, M.A.; Abdelaal, A.; Sojoudi, H. Surface Modification of Polymers: Methods and Applications. *Advanced Materials Interfaces* **2018**, *5*.
9. Chan, C.M.; Ko, T.M.; Hiraoka, H. Polymer Surface Modification by Plasmas and Photons. *Surface Science Reports* **1996**, *24*, 1–54, doi:10.1016/0167-5729(96)80003-3.
10. Mathieson, I.; Bradley, R.H. Improved Adhesion to Polymers by UV/Ozone Surface Oxidation. *International Journal of Adhesion and Adhesives* **1996**, *16*, 29–31, doi:10.1016/0143-7496(96)88482-X.
11. Koberstein, J.T. Molecular Design of Functional Polymer Surfaces. *Journal of Polymer Science, Part B: Polymer Physics* **2004**, *42*, 2942–2956, doi:10.1002/polb.20157.
12. Hariharan, A.; Kumar, S.K.; Russell, T.P. Surface Segregation in Binary Polymer Mixtures: A Lattice Model. *Macromolecules* **1991**, *24*, 4909–4917, doi:10.1021/ma00017a030.
13. Kumar, S.K.; Vacatello, M.; Yoon, D.Y. Off-Lattice Monte Carlo Simulations of Polymer Melts Confined between Two Plates. *The Journal of Chemical Physics* **1988**, *89*, 5206–5215, doi:10.1063/1.455611.
14. Hariharan, A.; Kumar, S.K.; Russell, T.P. Free Surfaces of Polymer Blends. II. Effects of Molecular Weight and Applications to Asymmetric Polymer Blends. *The Journal of Chemical Physics* **1993**, *99*, 4041, doi:10.1063/1.466100.
15. Tanaka, K.; Takahara, A.; Kajiyama, T. Surface Molecular Aggregation Structure and Surface Molecular Motions of High-Molecular-Weight Polystyrene/Low-Molecular-Weight Poly(Methyl Methacrylate) Blend Films. *Macromolecules* **1998**, *31*, 863–869, doi:10.1021/ma9709866.
16. Zhao, W.; Zhao, X.; Rafailovich, M.H.; Sokolov, J.; Composto, R.J.; Smith, S.D.; Satkowski, M.; Russell, T.P.; Dozier, W.D.; Mansfield, T. Segregation of Chain Ends to Polymer Melt Surfaces and Interfaces. *Macromolecules* **1993**, *26*, 561–562, doi:10.1021/ma00055a026.
17. Bitsanis, I.; Hadziioannou, G. Molecular Dynamics Simulations of the Structure and Dynamics of Confined Polymer Melts. *The Journal of Chemical Physics* **1990**, *92*, 3827, doi:10.1063/1.457840.
18. Minnikanti, V.S.; Archer, L.A. Entropic Attraction of Polymers toward Surfaces and Its Relationship to Surface Tension. *Macromolecules* **2006**, *39*, 7718–7728, doi:10.1021/ma061377d.
19. Kumar, S.K.; Vacatello, M.; Yoon, D.Y. Off-Lattice Monte Carlo Simulations of Polymer Melts Confined between Two Plates. *The Journal of Chemical Physics* **1988**, *89*, 5206–5215, doi:10.1063/1.455611.
20. Lee, H.; Archer, L.A. Functionalizing Polymer Surfaces by Field-Induced Migration of Copolymer Additives. 1. Role of Surface Energy Gradients. *Macromolecules* **2001**, *34*, 4572–4579.

21. Sabattié, E.F.D.; Tasche, J.; Wilson, M.R.; Skoda, M.W.A.; Hughes, A.; Lindner, T.; Thompson, R.L. Predicting Oligomer/Polymer Compatibility and the Impact on Nanoscale Segregation in Thin Films. *Soft Matter* **2017**, *13*, 3580–3591, doi:10.1039/C7SM00048K.
22. Zhu, S.; Hirt, D.E. Hydrophilization of Polypropylene Films by Using Migratory Additives. *Journal of Vinyl and Additive Technology* **2007**, *13*, 57–64, doi:10.1002/vnl.20102.
23. Lee, H.; Archer, L.A. Functionalizing Polymer Surfaces by Field-Induced Migration of Copolymer Additives - Role of Shear Fields. *Polymer Engineering and Science* **2002**, *42*, 1568–1579, doi:10.1002/pen.11052.
24. Zhu, S.; Hirt, D.E. Hydrophilization of Polypropylene Films by Using Migratory Additives. *Journal of Vinyl and Additive Technology* **2007**, *13*, 57–64, doi:10.1002/vnl.20102.
25. David, M.O.; Nipithakul, T.; Nardin, M.; Schultz, J.; Suchiva, K. Influence of Nonrubber Constituents on Tack of Natural Rubber. I. At Very Short Times of Contact (Pendulum Test). *Journal of Applied Polymer Science* **2000**, *78*, doi:10.1002/1097-4628(20001121)78:8<1486::AID-APP40>3.0.CO;2-I.
26. Datla, V.M.; Shim, E.; Pourdeyhimi, B. Polypropylene Surface Modification with Stearyl Alcohol Ethoxylates to Enhance Wettability. *Journal of Applied Polymer Science* **2011**, *121*, 1335–1347, doi:10.1002/app.31051.
27. Datla, V.M.; Shim, E.; Pourdeyhimi, B. Surface Modifications of Polypropylene with Nonylphenol Ethoxylates Melt Additives. *Polymer Engineering and Science* **2012**, *52*, 1920–1927, doi:10.1002/pen.23153.
28. Siqiang Zhu; Welsh, N.; Hirt, D.E. Determination of the Diffusivity of a Hydrophilic Migratory Additive in Ipp Films. *Journal of Plastic Film & Sheeting* **2007**, *23*, 187–201, doi:10.1177/8756087907084730.
29. Briddick, A.; J. Fong, R.; F. D. Sabattié, E.; Li, P.; W. A. Skoda, M.; Courchay, F.; L. Thompson, R. Blooming of Smectic Surfactant/Plasticizer Layers on Spin-Cast Poly(Vinyl Alcohol) Films. *Langmuir* **2018**, *34*, 1410–1418, doi:10.1021/acs.langmuir.7b04046.
30. Briddick, A.; Li, P.; Hughes, A.; Courchay, F.; Martinez, A.; Thompson, R.L. Surfactant and Plasticizer Segregation in Thin Poly(Vinyl Alcohol) Films. *Langmuir* **2016**, *32*, 864–872, doi:10.1021/acs.langmuir.5b03758.
31. Datla, V.M.; Shim, E.; Pourdeyhimi, B. Surface Modifications of Polypropylene with Nonylphenol Ethoxylates Melt Additives. *Polymer Engineering and Science* **2012**, *52*, 1920–1927, doi:10.1002/pen.23153.
32. Lu, J.R.; Hromadova, M.; Thomas, R.K.; Penfold, J. Neutron Reflection from Triethylene Glycol Monododecyl Ether Adsorbed at the Air-Liquid Interface: The Variation of the Hydrocarbon Chain Distribution with Surface Concentration. *Langmuir* **1993**, *9*, 2417–2425, doi:10.1021/la00033a026.
33. Campbell, R.A.; Saaka, Y.; Shao, Y.; Gerelli, Y.; Cubitt, R.; Nazaruk, E.; Matyszewska, D.; Lawrence, M.J. Structure of Surfactant and Phospholipid Monolayers at the Air/Water Interface Modeled from Neutron Reflectivity Data. *Journal of Colloid and Interface Science* **2018**, *531*, 98–108.
34. Carrascosa-Tejedor, J.; Santamaria, A.; Pereira, D.; Maestro, A. Structure of DPPC Monolayers at the Air/Buffer Interface: A Neutron Reflectometry and Ellipsometry Study. *Coatings* **2020**, *10*, 507.

35. Thomas, R.K.; Penfold, J. Neutron and X-Ray Reflectometry of Interfacial Systems in Colloid and Polymer Chemistry. *Current Opinion in Colloid and Interface Science* **1996**, *1*, 23–33.
36. Ma, G.; Barlow, D.J.; Hollinshead, C.M.; Harvey, R.D.; Webster, J.R.P.; Lawrence, M.J. Effects of Surface Pressure on the Structure of the Monolayer Formed at the Air/Water Interface by a Non-Ionic Surfactant. *Journal of Colloid and Interface Science* **2008**, *317*, 314–325, doi:10.1016/j.jcis.2007.09.011.
37. Penfold, J. Neutron Reflectivity and Soft Condensed Matter. *Current Opinion in Colloid and Interface Science* **2002**, *7*, 139–147, doi:10.1016/S1359-0294(02)00015-8.
38. Lu, J.R.; Hromadova, M.; Thomas, R.K.; Penfold, J. Neutron Reflection from Triethylene Glycol Monododecyl Ether Adsorbed at the Air-Liquid Interface: The Variation of the Hydrocarbon Chain Distribution with Surface Concentration. *Langmuir* **1993**, *9*, 2417–2425, doi:10.1021/la00033a026.
39. Litwinowicz, M.A.; Thompson, R.L.; Gibson, C.P. MUSCtR Available online: https://sourceforge.net/projects/musctr/.
40. Barradas, N.P.; Jeynes, C. Advanced Physics and Algorithms in the IBA DataFurnace. *Nuclear Instruments and Methods in Physics Research Section B: Beam Interactions with Materials and Atoms* **2008**, *266*, 1875–1879, doi:10.1016/j.nimb.2007.10.044.
41. Jeynes, C.; Barradas, N.P.; Szilágyi, E. Accurate Determination of Quantity of Material in Thin Films by Rutherford Backscattering Spectrometry. *Analytical Chemistry* **2012**, *84*, 6061–6069, doi:10.1021/ac300904c.
42. Stalder, A.F.; Kulik, G.; Sage, D.; Barbieri, L.; Hoffmann, P. A Snake-Based Approach to Accurate Determination of Both Contact Points and Contact Angles. *Colloids and Surfaces A: Physicochemical and Engineering Aspects* **2006**, *286*, 92–103, doi:10.1016/j.colsurfa.2006.03.008.
43. Kuhn, H.; Rehage, H. Molecular Orientation of Monododecyl Pentaethylene Glycol (C12E5) Surfactants at Infinite Dilution at the Air/Water Interface. A Molecular Dynamics Computer Simulation Study. *Physical Chemistry Chemical Physics* **2000**, *2*, 1023–1028, doi:10.1039/a906992e.
44. Fong, R.J.; Squillace, O.; Reynolds, C.D.; Cooper, J.F.K.; Dalgliesh, R.M.; Tellam, J.; Courchay, F.; Thompson, R.L. Segregation of Amine Oxide Surfactants in PVA Films. *Langmuir* **2020**, *36*, doi:10.1021/acs.langmuir.0c00084.
45. Wahlgren, M.; Kedström, J.; Arnebrant, T. The Interactions in Solution between Nonionic Surfactants and Globular Proteins: Effects on Cloud Point. *Journal of Dispersion Science and Technology* **1997**, *18*, 449–458, doi:10.1080/01932699708943747.
46. Briddick, A.; Li, P.; Hughes, A.; Courchay, F.; Martinez, A.; Thompson, R.L. Surfactant and Plasticizer Segregation in Thin Poly(Vinyl Alcohol) Films. *Langmuir* **2016**, *32*, 864–872, doi:10.1021/acs.langmuir.5b03758.
47. Lee, L.-H. Adhesion of High Polymers. II. Wettability of Elastomers. *Journal of Polymer Science Part A-2: Polymer Physics* **1967**, *5*, 1103–1118, doi:10.1002/pol.1967.160050610.
48. Wu, S. Estimation of the Critical Surface Tension for Polymers from Molecular Constitution by a Modified Hildebrand-Scott Equation. *Journal of Physical Chemistry* 1968.
49. van Oss, C.J.; Chaudhury, M.K.; Good, R.J. Monopolar Surfaces. *Advances in Colloid and Interface Science* **1987**, *28*, 35–64, doi:10.1016/0001-8686(87)80008-8.

50. van Krevelen, D.W.; Hoftyzer *Properties of Polymers: Their Estimation and Correlation with Chemical Structure*; 2nd ed.; Elsevier: Amsterdam, The Netherlands, 1976;
51. Xie, W.; Weng, L.T.; Yeung, K.L.; Chan, C.M. Segregation of Dioctyl Phthalate to the Surface of Polystyrene Films Characterized by ToF-SIMS and XPS. *Surface and Interface Analysis* **2018**, *50*, 1302–1309.
52. Garza, C.; Thieghi, L.T.; Castillo, R. Atomic Force Microscopy Images of Lyotropic Lamellar Phases. *Journal of Chemical Physics* **2007**, *126*, 051106, doi:10.1063/1.2483389.
53. Dong, J.; Mao, G. Direct Study of C 12 E 5 Aggregation on Mica by Atomic Force Microscopy Imaging and Force Measurements. *Langmuir* **2000**, *16*, 6641–6647, doi:10.1021/la000103v.
54. Shirai, S.; Einaga, Y. Wormlike Micelles of Polyoxyethylene Dodecyl C12Ej and Heptaoxyethylene Alkyl CiE7 Ethers. Hydrophobic and Hydrophilic Chain Length Dependence of the Micellar Characteristics. *Polymer Journal* **2005**, *37*, doi:10.1295/polymj.37.913.
55. Xie, W.; Weng, L.T.; Yeung, K.L.; Chan, C.M. Segregation of Dioctyl Phthalate to the Surface of Polystyrene Films Characterized by ToF-SIMS and XPS. *Surface and Interface Analysis* **2018**, *50*, 1302–1309.
56. Sabattié, E.F.D.; Tasche, J.; Wilson, M.R.; Skoda, M.W.A.; Hughes, A.; Lindner, T.; Thompson, R.L. Predicting Oligomer/Polymer Compatibility and the Impact on Nanoscale Segregation in Thin Films. *Soft Matter* **2017**, *13*, 3580–3591, doi:10.1039/C7SM00048K.